Supporting Information for "Influence of erosive fluidization on the morphology of fluid flow and escape structures"

S. Gupta[1]and A. Micallef[1,2]

[1]Helmholtz Center for Ocean Research GEOMAR, Kiel, Germany

[2]Department of Geosciences, University of Malta, Msida, Malta

Contents of this file

1. Figures S1 to S3

Additional Supporting Information (Files uploaded separately)

1. Captions for Movies S1 to S2

Introduction

Our simulation results show how flow of pressurized gas causes erosion of the sediment and subsequent fluidization, transport, and resettlement of the eroded soil particles. Distinct focused flow pathways open up in the sub-surface, which manifest as pockmarks at the seafloor. For a given geological setting, the shape of the flow pathways and the

Corresponding author: S. Gupta, Helmholtz Center for Ocean Research GEOMAR, Kiel, Germany. (sgupta@geomar.de)

pockmarks is controlled by the local anisotropy (i.e., $K_F := \frac{K_{0,0}}{K_{0,1}}$) and the relative erodibility (i.e., $r_0 := \frac{e_0}{ds_0}$) of the sediment. Selected results presented in the main manuscript (Figures 2 and 3) show 1) conical focused flow conduits with brecciated core and annular gas channels encased within a halo of low permeability sediment; 2) pockmarks of diverse shapes and sizes on the seafloor, including W-, U-, and ring-shapes; and 3) a pulsed release of gas. To further support the main results, we present, in **Figure S1**, **Figure S2**, and **Figure S3** the snapshots of numerical results for *all* simulations corresponding to the scenario with $K_{0,1} = 10^{-13}$ m^2 (that was used as a reference case in the manuscript, specified in Figure 1-C).

We also show animations (uploaded separately) of two particular scenarios 1) **Movie S1** with $K_{0,1} = 10^{-13}m^2$, $K_F = 1$, $r_0 = 50$; and 2) **Movie S2** with $K_{0,1} = 10^{-13}m^2$, $K_F = 10$, $r_0 = 100$. These animations show the initiation and propagation of flow localization in the subsurface and formation of pockmarks on the seafloor. They also show the gas pulses and the annular flow of gas in the pipe/chimney regions.

Figure S1. Figure shows the snapshot of the redistributed sediment (i.e., volume of fluidized as well as bound soil per unit REV, $s := (1-\phi) + \frac{\rho_s}{\rho_w}\phi S_w \overline{\Theta}_f$) for the test scenario with $K_{0,1} = 10^{-13}$ m^2. The snapshot corresponds to time $t = 2$ years, and shows the variation in the shapes and sizes of pipes/chimneys and pockmarks with respect to sediment anisotropy $K_F \in \{1, 10, 100\}$ and relative erodibility $r_0 \in \{100, 50, 25\}$. On the sea-floor, high r_0 and low K_F lead to ring-like pockmarks (e.g. (a), (b)), while low r_0 and high K_F lead to shallow U-shaped pockmarks (e.g. (h), (i)). In general, though, active fluid escape leads to W-shaped pockmarks (e.g., (c)-(g)) with different depths, gradients, and lateral extent. In the sub-surface, gas flow leads to a conical focused-flow pathway (dark-blue zone), encased in a 'halo' of high sediment fraction (white zone) which obstructs lateral fluxes, leading to flow-localization. High r_0 and low K_F lead to sharper focused-flow pathways with tight sediment halos (i.e. pipes, e.g., (a), (b)), while low r_0 and high K_F lead to more diffuse focused-flow pathways without sharp boundaries with the sediment halos (or chimneys, e.g. (f), (h), (i)).

Figure S2. Figure shows the snapshot of the redistributed sediment (i.e., volume of fluidized as well as bound soil per unit pore-water, $s\prime := \frac{s}{S_w}$) for the test scenario with $K_{0,1} = 10^{-13}$ m^2. The snapshots correspond to time $t = 2$ years, and highlight the gas-flow channels within the pipes/chimneys (i.e., since fluidized sediment particles are suspended only in water, by dividing with S_w, we can identify preferential gas paths). The snapshots show the variation of channels with respect to sediment anisotropy $K_F \in \{1, 10, 100\}$ and relative erodibility $r_0 \in \{100, 50, 25\}$. Sharpness of the gas channels reduces mainly with decreasing r_0, and to a lesser extent, with increasing K_F. The sharpness of the gas channels shows strong correlating with the depth and gradient of the pockmarks, and their transition from ring- to W- to U-shapes.

Figure S3. Figure shows snapshots of the gas saturation S_n for the test scenario with $K_{0,1} = 10^{-13}\,\mathrm{m}^2$ with respect to sediment anisotropy $K_F \in \{1, 10, 100\}$ and relative erodibility $r_0 \in \{100, 50, 25\}$. The snapshots correspond to time $t = 2$ years. Gas ascent occurs in pulses, where the frequency of gas pulses increases with increasing K_F and decreasing $r_0 := \frac{e_{n,0}}{ds_{w,0}}$.

Movie S1. Movie shows evolution over time of A) gas saturation S_n, B) gas mass flux (orange vectors) $\mathbf{F} := \rho_n \mathbf{v}_n$, and C) redistributed sediment $s := (1-\phi) + \frac{\rho_s}{\rho_w}\phi S_w \overline{\Theta}_f$, for the scenario with $K_{0,1} = 10^{-13} m^2$, $K_F = 1$, $r_0 = 50$. The profile (A) shows the gas pulses, and (C) shows the evolution of the conical focused flow path and sediment halo in the subsurface, as well as a W-shaped pockmark on the seafloor. In profile (B), the gas flux vectors (in orange) are superimposed over the redistributed sediment (blue-to-white in the background). In particular, (B) highlights the annular gas flow within the focused flow path.

Movie S2. Movie shows evolution over time of A) gas saturation S_n, B) gas mass flux (orange vectors) $\mathbf{F} := \rho_n \mathbf{v}_n$, and C) redistributed sediment $s := (1-\phi) + \frac{\rho_s}{\rho_w}\phi S_w \overline{\Theta}_f$, for the scenario with $K_{0,1} = 10^{-13} m^2$, $K_F = 10$, $r_0 = 100$. The profile (A) shows the gas pulses, and (C) shows the evolution of the conical focused flow path and sediment halo in the subsurface, as well as a complex ring-shaped pockmark on the seafloor. In profile (B), the gas flux vectors are superimposed over the redistributed sediment (in the background). (B) highlights the annular gas flow within the focused flow path.

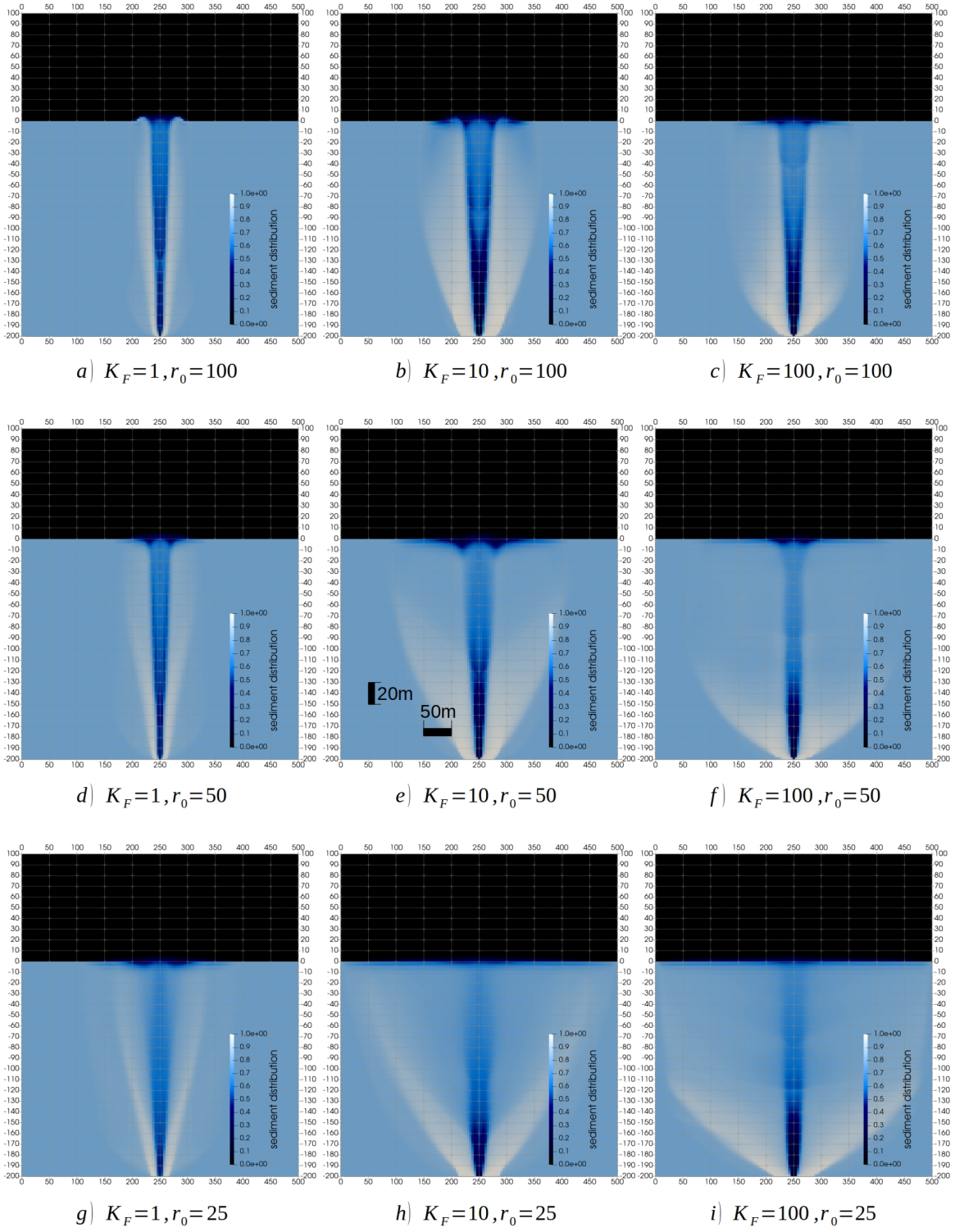

a) $K_F=1, r_0=100$ b) $K_F=10, r_0=100$ c) $K_F=100, r_0=100$

d) $K_F=1, r_0=50$ e) $K_F=10, r_0=50$ f) $K_F=100, r_0=50$

g) $K_F=1, r_0=25$ h) $K_F=10, r_0=25$ i) $K_F=100, r_0=25$

Figure S1. Snapshots of the redistributed sediment $s := (1-\phi) + \frac{\rho_s}{\rho_w}\phi S_w \overline{\Theta}_f$ (i.e., volume of fluidized as well as bound soil per unit REV) for the test scenario with $K_{0,1} = 10^{-13}$ m^2.

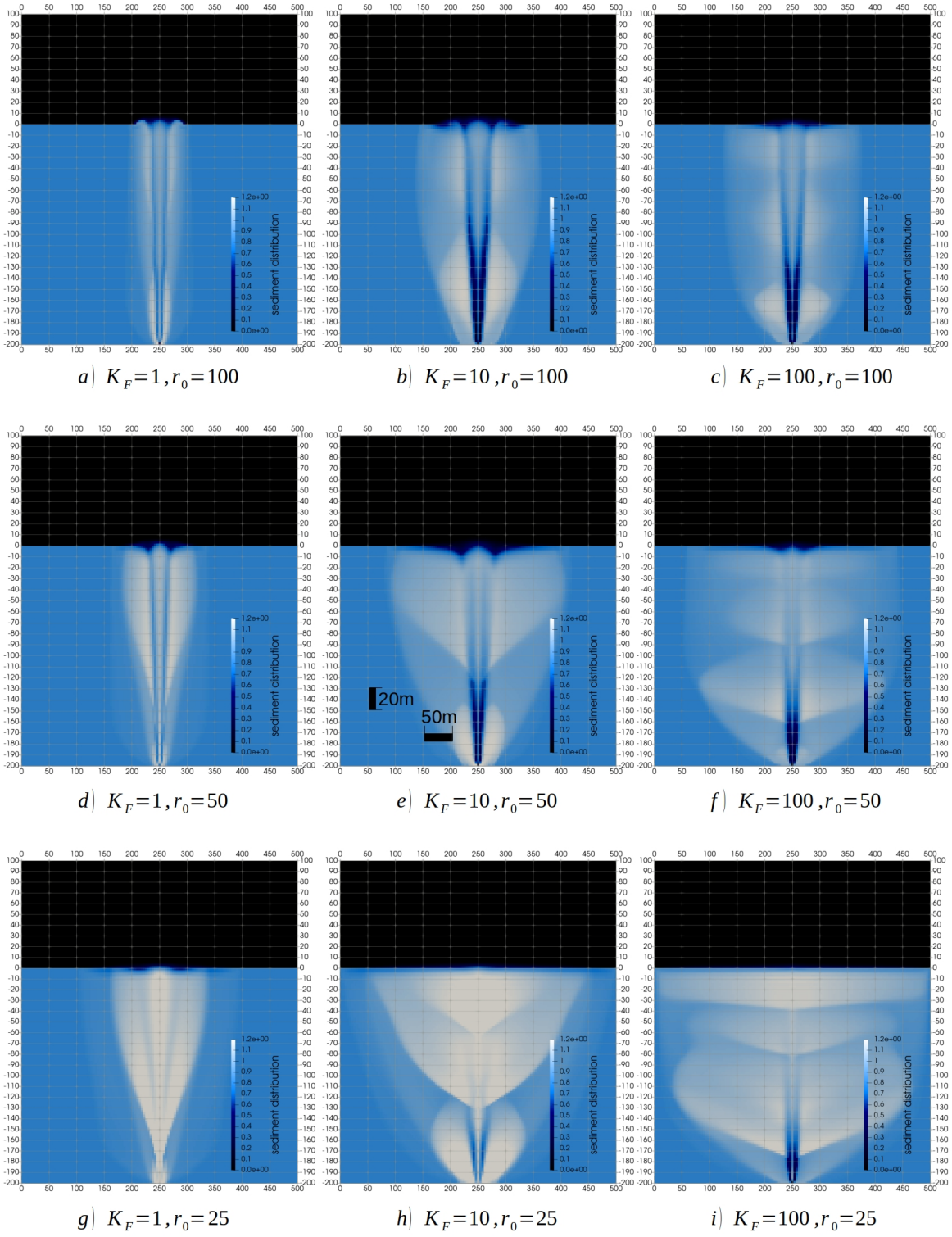

a) $K_F=1, r_0=100$ b) $K_F=10, r_0=100$ c) $K_F=100, r_0=100$

d) $K_F=1, r_0=50$ e) $K_F=10, r_0=50$ f) $K_F=100, r_0=50$

g) $K_F=1, r_0=25$ h) $K_F=10, r_0=25$ i) $K_F=100, r_0=25$

Figure S2. Snapshots of the redistributed sediment $s\prime := \frac{s}{S_w}$ (i.e., volume of fluidized as well as bound soil per unit pore-water) for the test scenario with $K_{0,1} = 10^{-13}$ m^2.

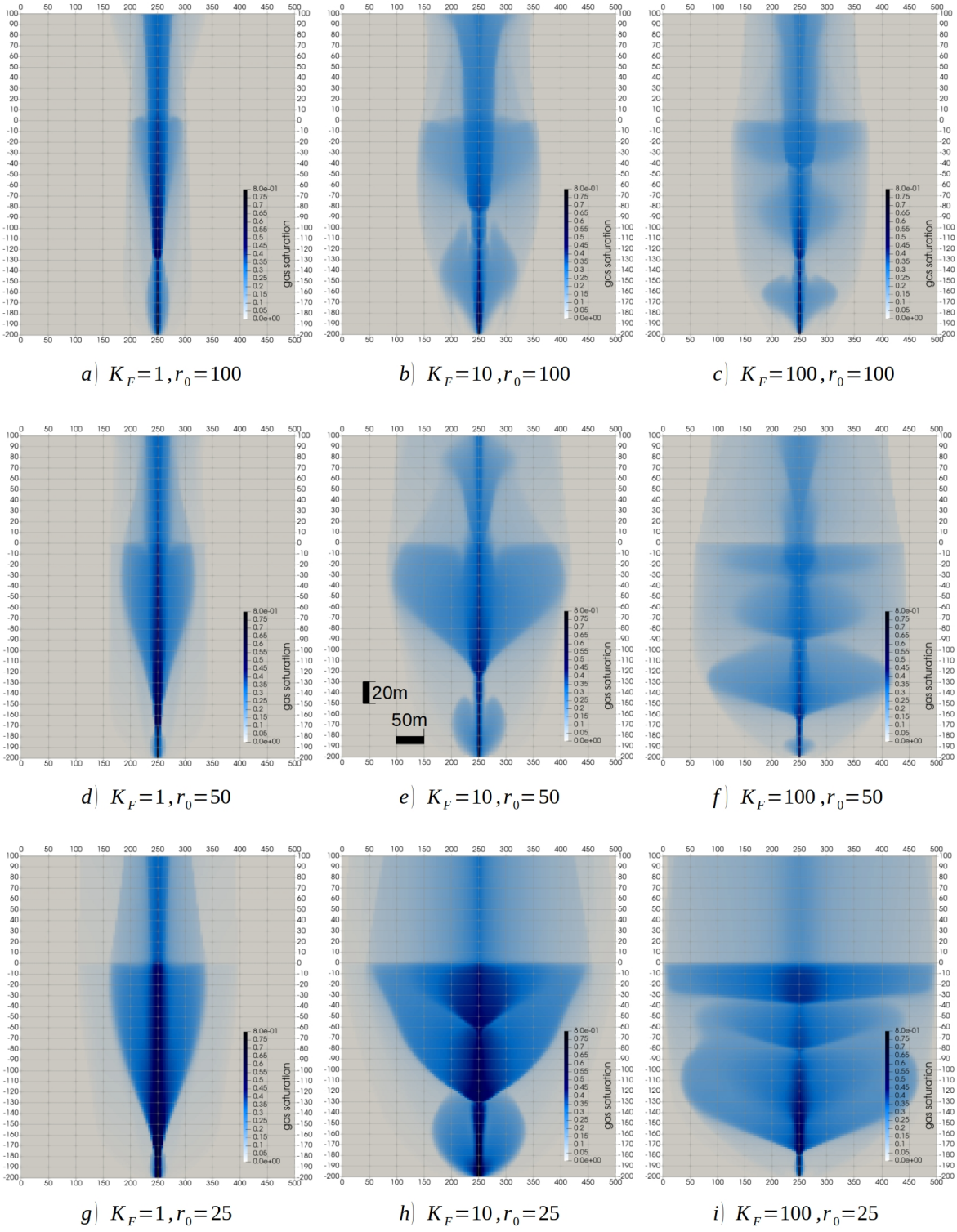

a) $K_F=1, r_0=100$ b) $K_F=10, r_0=100$ c) $K_F=100, r_0=100$

d) $K_F=1, r_0=50$ e) $K_F=10, r_0=50$ f) $K_F=100, r_0=50$

g) $K_F=1, r_0=25$ h) $K_F=10, r_0=25$ i) $K_F=100, r_0=25$

Figure S3. Snapshots of the gas saturation S_n for the test scenario with $K_{0,1} = 10^{-13}$ m^2.